A Wireless Charging System Applying Phase-Shift and Amplitude Control to Maximize Efficiency and Extractable Power

Andreas Berger, Matteo Agostinelli, Sanna Vesti, Jesús A. Oliver, José A. Cobos and Mario Huemer

***Abstract*—Wireless power transfer (WPT) is an emerging technology with an increasing number of potential applications to transfer power from a transmitter to a mobile receiver over a relatively large air gap. However, its widespread application is hampered due to the relatively low efficiency of current Wireless power transfer (WPT) systems. This study presents a concept to maximize the efficiency as well as to increase the amount of extractable power of a WPT system operating in nonresonant operation. The proposed method is based on actively modifying the equivalent secondary-side load impedance by controlling the phase-shift of the active rectifier and its output voltage level. The presented hardware prototype represents a complete wireless charging system, including a dc–dc converter which is used to charge a battery at the output of the system. Experimental results are shown for the proposed concept in comparison to a conventional synchronous rectification approach. The presented optimization method clearly outperforms state-of-the-art solutions in terms of efficiency and extractable power.**

***Index Terms*—Dc-dc power converters, impedance matching, inductive power transmission, phase-shift control, reactive power control, rectifiers, wireless charging.**

I. Introduction

WIRELESS power transfer (WPT) is used in various application fields ranging from a few milliwatts in biomedical applications [1]–[3] up to several kilowatts of output power in automotive applications [4]–[6]. Currently, WPT systems intended to wirelessly charge consumer electronic devices, such as mobile phones or tablet computers, are studied extensively [7]–[10]. Various aspects of these systems are defined by several standards which are either based on nonresonant or inductive power transfer (IPT), like the Qi standard [11] or on resonant power transfer (RPT), like the Rezence standard [12]. In order to ensure interoperability of different transmitter and receiver devices, these standards define parameters such as the voltage range, the basic circuit structure, and the operating frequency of the system. The main drawbacks of currently available WPT systems for consumer applications are, amongst others, the relatively low overall efficiency and the limited power transfer capability. This results in long charging times which hampers the widespread application of the WPT technology.

To overcome these problems, various improvements have been suggested in the literature. Design and optimization methodologies for increasing the efficiency or the maximum transferable power of a WPT link have been proposed in [13]–[16], assuming that the system parameters are freely selectable. However, these optimization strategies are not applicable to commercial charging applications, where the system parameters are defined by a standard.

On the other hand, various optimization methods which are in accordance with current standards are reported. In [17], different control strategies for the transmitter of a WPT system are compared regarding their impact on the output power and the efficiency. Furthermore, in [18], a control scheme for a synchronous rectifier on the secondary side is proposed to improve the efficiency in comparison to a passive and semiactive rectifier solution.

Although WPT has been extensively studied in recent years, less attention has been paid to the optimization of an entire wireless charging system, starting from a dc input source to charging a battery at the output. In [19], a Qi compliant wireless charging system has been presented but only commercial available components have been used and no advanced optimization techniques have been applied to increase the system efficiency and the extractable output power. In [9], a dual mode receiver architecture is presented which is capable of operating according to the Qi standard (110–205 kHz) and the Rezence standard (6.78 MHz). Experimental results, from the input of the rectifier to the battery at the output, show a higher efficiency for the nonresonant operating mode mainly due to lower switching losses.

In a wireless charging system the efficiency and the amount of power transferred to the output are influenced by the source (transmitter) and load (receiver) impedances. In [20], the load impedance is assumed to be purely resistive and, therefore, efficiency improvements are reported by only adjusting the resistive part of the load impedance. However, this approach does not yield optimal efficiency for the whole operating range, since only the resistive part of the load impedance is altered and the

reactive part is not considered at all. The maximum amount of power can be transferred by modifying the load impedance to match the complex conjugate of the source impedance [21]. An impedance adjustment unit is applied in [22] to cancel the reactive part of the impedance and thereafter to alter the resistive part in order to yield maximum power transfer. Yet, this technique uses a network of passive components to adjust the impedance, and it targets only to achieve the maximum extractable output power while the system efficiency is not optimized. Additional improvements to the efficiency of a WPT system are obtained by actively modifying the reactive part of the load impedance. In [23], a phase-shift control approach, instead of a conventional controlling method, is applied to the active rectifier on the secondary side of an RPT system. This technique is used to achieve efficiency improvements by modifying the secondary-side resonance frequency, but on the other hand it also impacts the equivalent load impedance. Since the phase-shift is the only control parameter, the resistive as well as the reactive part of the equivalent load impedance are concurrently altered. Hence, these two parameters cannot be controlled separately and the point of maximum efficiency is not reached in general. Furthermore, it might be highlighted that [23] solely investigates an RPT system with a resistive load at the output of the rectifier.

In this study, an advanced optimization strategy for an entire wireless charging system, including an active rectifier and a dc–dc converter charging a battery, is investigated in detail. The presented approach assumes nonresonant operation (IPT) and is based on the Qi standard specifications. When applied to an RPT system operating exactly at resonance frequency, the reactive part of the system is inherently compensated, and hence the proposed approach shows the same behavior as a synchronous rectifier. However, any deviation from the resonance frequency, caused, e.g., by parameter variations of the passive components, enables a performance increase of the proposed concept over a synchronous rectification approach. An improved control strategy to actively adjust the resistive as well as the reactive part of the equivalent load impedance is introduced in order to optimize the system performance. This approach, applicable to any IPT system, is used to further improve the system efficiency and to extract more power. The presented methodology is based on controlling both the phase-shift of the active rectifier and its output voltage level. This study is an extension to the concept we proposed in [24], where only a simplified system has been investigated and a voltage source at the output of the rectifier is used to set a desired voltage level. In contrast, this paper investigates a complete wireless charging system, including a dc–dc converter to regulate the rectified voltage and a battery as load of the system. The acquired simulations and experimental results show that the proposed concept is capable of achieving significant performance improvements in terms of efficiency and extractable power when compared to prior solutions.

The remainder of this paper is organized as follows: In Section II, the theoretical background of the presented methodology is derived and thereafter in Section III the proposed concept is discussed in detail. In Section IV, the applied optimization strategy is introduced and in Section V the architecture of the investigated wireless charging system as well as experimental results acquired from the WPT prototype are presented. Finally, in Section VI the major findings of this study are summarized and concluding remarks are given.

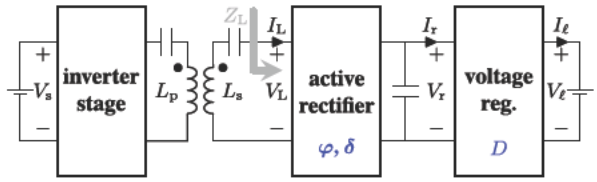

Fig. 1. Schematic block diagram of the overall WPT system including an inverter stage driving the primary side resonance circuit, an active rectifier and a dc–dc converter at the secondary side.

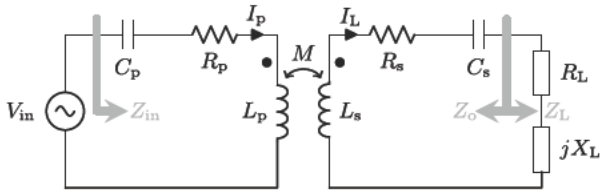

Fig. 2. Equivalent circuit model of a series-series tuned WPT system based on the first harmonic approximation.

II. Theoretical Analysis

In this section, the methodology for modeling the behavior of the WPT system is introduced and the theoretical conditions for calculating the maximum efficiency and the maximum power transfer are provided. This study focuses on a circuit-based model, but it is worth noting that there exist different other possibilities to model WPT systems [13], [25], [26]. A block diagram of the examined system is shown in Fig. 1.

A. System Modeling

The first harmonic approximation is used to analyze the WPT system shown in Fig. 1. This method only considers the fundamental component of the input voltage [15], [25], [27] and replaces the active rectifier as well as the dc–dc converter by an equivalent first harmonic impedance $Z_L = R_L + jX_L$. The applied simplification is sufficiently accurate for high quality factor resonant circuits that operate near resonance frequency. This study focuses on the steady-state analysis of a series-series resonant WPT system as shown in Fig. 2, but the proposed concept is applicable to every topology.

The sinusoidal voltage source V_{in} is an equivalent root mean square (RMS) input voltage which is driving the primary side resonance circuit. The series resistances R_p and R_s represent the overall parasitic resistances of the primary and the secondary side resonance circuit. The series capacitors C_p and C_s are required to tune the resonance frequency of the primary and the secondary side, while the mutual inductance M depends on the coupling factor $k = M\sqrt{L_p L_s}$, which is influenced by the geometry, the distance, and the alignment of the inductors

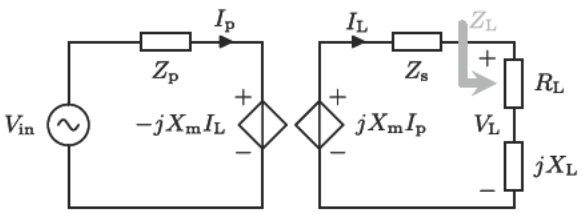

Fig. 3. Circuit model of the WPT system using two equivalent sources to model the coupling between the inductors L_p and L_s.

L_p and L_s. The open-circuit impedances of the primary and secondary side resonance circuits are defined as

$$Z_\mathrm{p} = R_\mathrm{p} + jX_\mathrm{p} = R_\mathrm{p} + j\left(\omega L_\mathrm{p} - \frac{1}{\omega C_\mathrm{p}}\right) \tag{1}$$

$$Z_\mathrm{s} = R_\mathrm{s} + jX_s = R_s + j\left(\omega L_\mathrm{s} - \frac{1}{\omega C_s}\right). \tag{2}$$

The equivalent load impedance of the WPT system can be modeled as a complex impedance $Z_\mathrm{L} = R_\mathrm{L} + jX_\mathrm{L}$, which represents the overall impedance seen by the secondary side resonance circuit, including the rectifier, the dc–dc converter and the battery at the output of the system. The impedances Z_in and Z_o, as shown in Fig. 2, are the equivalent impedances seen by the source and by the output, respectively. They can be expressed as

$$Z_\mathrm{in} = Z_\mathrm{p} + \frac{X_\mathrm{m}^2}{Z_\mathrm{s} + Z_\mathrm{L}} \tag{3}$$

$$Z_\mathrm{o} = Z_\mathrm{s} + \frac{X_\mathrm{m}^2}{Z_\mathrm{p}} \tag{4}$$

where $X_\mathrm{m} = \omega M$ represents the mutual impedance of the coupled inductors. To further simplify the ac circuit model in Fig. 2, the coupled inductors L_p and L_s can be modeled as equivalent current controlled voltage sources at the primary and the secondary side as shown in Fig. 3.

The induced voltage at the secondary side is influenced by the primary side current I_p and can be denoted by $jX_\mathrm{m}I_\mathrm{p}$. On the other hand, the current at the secondary side I_L also causes an induced voltage at the primary side inductor which is determined by $-jX_\mathrm{m}I_\mathrm{L}$. Furthermore, V_in represents the input and V_L the output voltage, and I_p the input and I_L the output current of the system. The impedances Z_p and Z_s are defined according to (1) and (2).

B. *Efficiency and Extractable Power*

In order to analyze the system performance, the input and output power of the WPT system are derived as a function of the resistive part R_L and the reactive part X_L of the equivalent load impedance. The following relations for the mean input power P_in, respectively the mean output power P_out, are based on the equivalent model in Fig. 3 and are given as

TABLE I
SUMMARY OF THE POSSIBILITIES TO OPTIMIZE THE EQUIVALENT LOAD IMPEDANCE OF A WPT SYSTEM

Load Impedance	Optimization Concept
$Z_\mathrm{L} = R_\mathrm{L} + j0$	synchronous rectification (purely resistive behavior)
$Z_\mathrm{L} = R_\mathrm{L} - jX_s$	single point optimization (cancelation of reactive part)
$Z_\mathrm{L} = R_\mathrm{o} - jX_\mathrm{o} = Z_\mathrm{o}^*$	maximum power transfer approach (conjugate matching)
$Z_\mathrm{L} = R_\mathrm{L}(\varphi) + jX_\mathrm{L}(\varphi)$	pure phase-shift (no independent adjustment of R_L and X_L)
$Z_\mathrm{L} = R_\mathrm{L}(\varphi, V_\mathrm{r}) - jX_\mathrm{L}(\varphi, V_\mathrm{r})$	proposed approach (separate adjustment of R_L and X_L)

$$P_\mathrm{in}(R_\mathrm{L}, X_\mathrm{L}) = \frac{V_\mathrm{in}^2\left[R_\mathrm{p} + \mathrm{Re}\left\{Z_\mathrm{r}\right\}\right]}{\left[R_\mathrm{p} + \mathrm{Re}\left\{Z_\mathrm{r}\right\}\right]^2 + \left[X_\mathrm{p} + \mathrm{Im}\left\{Z_\mathrm{r}\right\}\right]^2} \tag{5}$$

$$P_\mathrm{out}(R_\mathrm{L}, X_\mathrm{L}) = \frac{V_\mathrm{in}^2 X_\mathrm{m}^2 R_\mathrm{L}}{\mathrm{den}} \tag{6}$$

where

$$\mathrm{den} = \left[R_\mathrm{p}\left(R_\mathrm{s} + R_\mathrm{L}\right) - X_\mathrm{p}\left(X_\mathrm{s} + X_\mathrm{L}\right) + X_\mathrm{m}^2\right]^2 + \left[X_\mathrm{p}\left(R_\mathrm{s} + R_\mathrm{L}\right) + R_\mathrm{p}\left(X_\mathrm{s} + X_\mathrm{L}\right)\right]^2$$

and V_in denotes the RMS value of the input voltage of the system. The impedance Z_r represents the reflected impedance from the secondary to the primary side which can be derived as

$$Z_\mathrm{r} = \frac{X_\mathrm{m}^2}{Z_\mathrm{s} + Z_\mathrm{L}}. \tag{7}$$

It is well known from the literature that the maximum output power can be achieved by a conjugate matching of the equivalent load and output impedance of the system ($Z_\mathrm{L} = Z_\mathrm{o}^*$) [14], [21].

With the relations (5) and (6) for the input and output power, the system efficiency as a function of the load impedance can be expressed as

$$\eta(R_\mathrm{L}, X_\mathrm{L}) = \frac{X_\mathrm{m}^2 R_\mathrm{L}}{R_\mathrm{p}\left[\left(R_\mathrm{s} + R_\mathrm{L}\right)^2 + \left(X_\mathrm{s} + X_\mathrm{L}\right)^2\right] + X_\mathrm{m}^2\left(R_\mathrm{s} + R_\mathrm{L}\right)}. \tag{8}$$

In case only the efficiency is considered, (8) can be maximized by canceling the reactive part ($X_\mathrm{L} = -X_s$) and by solely optimizing the real part R_L of the equivalent load. The optimal load resistance can then be derived by setting the derivative of (8) to zero which yields [25]

$$R_\mathrm{L,opt} = \sqrt{R_\mathrm{s}^2 + \frac{R_\mathrm{s}}{R_\mathrm{p}} X_\mathrm{m}^2}. \tag{9}$$

This approach is referred to as single-point efficiency optimization in the following, since it maximizes the efficiency only for a

TABLE II
SUMMARY OF THE MAIN SYSTEM PARAMETERS

	Parameter	Symbol	Value
	input voltage	V_s	19 V
general	coupling factor	k	0.6/0.3
parameters	resonance frequency	f_{res}	100 kHz
	operating frequency	f_{op}	140 kHz
primary	inductor	L_{p}	24 μH
side	resonance capacitor	C_{p}	93 nF
secondary	inductor	L_{s}	10 μH
side	resonance capacitor	C_{s}	242 nF
dc–dc	inductor	L	1 μH
parameters	capacitor	C	10 μF
battery	nominal voltage	V_ℓ	3.8 V
parameters	series resistance	R_{Bat}	70 mΩ

single value of the output power which can be far from the maximum output power of the system. If the output power is varied by altering the load resistance R_{L}, the efficiency decreases and the system does not operate at the optimum efficiency for this particular value of the output power. It is worth noting that the conditions ($R_{\text{L}} = R_{\text{L,opt}}, X_{\text{L}} = -X_{\text{s}}$) for maximum efficiency, and ($Z_{\text{L}} = Z_{\text{o}}^*$) for maximum power transfer are in general not fulfilled at the same time. To overcome these drawbacks and to achieve optimum efficiency for every possible value of output power, an optimization method is required to adjust both the resistive and the reactive part of the equivalent load impedance.

III. Proposed Concept

In this section synchronous rectification is briefly reviewed and, thereafter, the proposed concept for controlling the equivalent load impedance to optimize the efficiency and to increase the power transfer capability is discussed in detail. Simulation results are shown for a WPT system based on the Qi low-power specifications, operating at a frequency of 140 kHz with a resonance frequency of 100 kHz. The values used for simulation are based on the parameters of the experimental setup which are summarized in Table II in Section V.

A. Synchronous Rectification

Synchronous rectification is a commonly used technique to control an active rectifier, where the switches of the full bridge are driven according to the zero crossings of the rectifier input current I_{L}. Thus, the controller forces the current I_{L} and the voltage V_{L} at the input of the rectifier to be in phase ($\varphi = 0$), which results in a purely resistive behavior of the rectifier without compensation of the reactive part ($Z_{\text{L}} = R_{\text{L}} + j0$). Fig. 4 schematically illustrates the key waveforms of the synchronous rectification approach. To obtain the maximum efficiency for every point of the output power P_{out} the rectified voltage V_{r} is adjusted by controlling the duty cycle D of the dc–dc converter.

B. Proposed Concept

Recent research [23] has shown the possibility to improve the performance of a WPT system by introducing a phase-shift

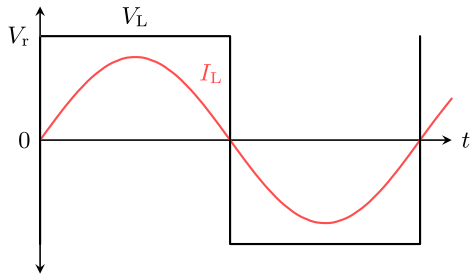

Fig. 4. Rectifier input voltage V_{L} and current I_{L} for synchronous rectification ($\varphi = 0$).

between the primary and secondary side voltages. However, this method does not allow to separately control the resistive and reactive part of the equivalent load impedance, whereas in the proposed concept the overall impedance is controlled. By defining the phase-shift φ as the angle between the first harmonic of the input current I_{L} and the voltage V_{L} of the active rectifier we derived an analytical expression for the equivalent input impedance of the active rectifier [24]

$$\begin{aligned} Z_{\text{L}}(\varphi, V_{\text{r}}) = \; & R_{\text{L}} + jX_{\text{L}} = \frac{V_{\text{L}}^{(1)}}{I_{\text{L}}^{(1)}} = \frac{4}{\pi}\frac{V_{\text{r}}}{I_{\text{L}}^{(1)}} e^{-j\varphi} \\ = \; & \frac{4}{\pi}\frac{V_{\text{r}}}{I_{\text{L}}^{(1)}} \left(\cos(\varphi) - j\sin(\varphi)\right) \end{aligned} \tag{10}$$

where $V_{\text{L}}^{(1)}$ and $I_{\text{L}}^{(1)}$ represent the amplitude of the first harmonic of the voltage V_{L} and the current I_{L}. By analyzing (10), it can be observed that a variation in the phase results in a change of the resistive as well as the reactive part of the equivalent load impedance. This behavior limits the optimization possibilities in case only the phase is actively controlled. On the other hand (10) shows the possibility to further improve the system by modifying a second parameter, the rectified voltage V_{r}. This parameter can be controlled by either altering the duty cycle δ of the active rectifier or by adjusting the voltage regulator at the output of the system. Fig. 5(a) schematically illustrates the phase-shift concept using the duty cycle D of the dc–dc converter to adjust the rectified voltage V_{r}, and Fig. 5(b) shows the phase-shift and duty cycle δ control method for the active rectifier. It is worth noting that these waveforms are schematic illustrations and do not yield the same equivalent resistance R_{L} for the shown case.

By correctly adjusting D or δ the same value of rectified voltage V_{r} and hence the same equivalent resistance R_{L} can be achieved. The fundamental component of the rectifier input voltage V_{L} for the case of the duty cycle D control [see Fig. 5(a)] and the δ control [see Fig. 5(b)] can be denoted by

$$V_{\text{L}}^{(1)}(\varphi, D) = \frac{4}{\pi} V_{\text{r}} e^{-j\varphi} = \frac{4}{\pi}\frac{V_\ell}{D} e^{-j\varphi} \tag{11}$$

$$V_{\text{L}}^{(1)}(\varphi, \delta) = \frac{4}{\pi} V_{\text{r}} \sin\left(\delta/2\right) e^{-j\varphi} \tag{12}$$

where $0 \leq D \leq 1$ and $0 \leq \delta \leq \pi$. Consequently, both of the presented control approaches can be used to regulate the rectified

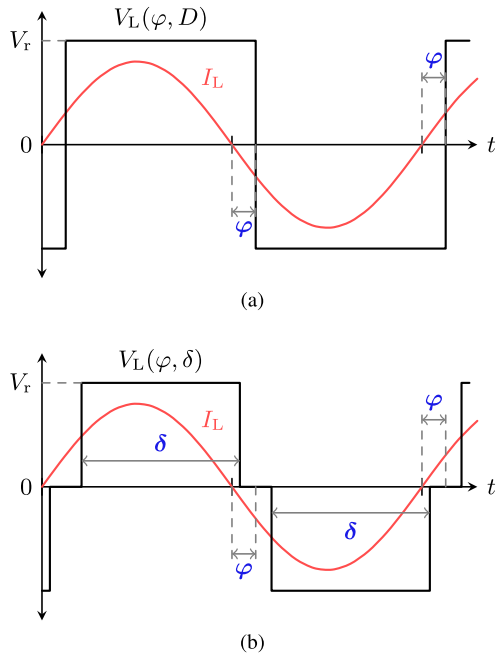

Fig. 5. Schematic illustration of the key waveforms of the proposed method. (a) Voltage V_L and current I_L at the input of the rectifier utilizing the duty cycle D of the dc–dc converter to control the amplitude of the rectified voltage V_r. (b) Voltage V_L and current I_L at the input of the rectifier using the duty cycle δ of the active rectifier to adjust the rectified voltage V_r.

voltage V_r, but in this study the impact of the duty cycle D of the employed dc–dc converter is investigated in detail. The relation between the voltage regulator input (V_r) and output voltage (V_ℓ) affects the resistive part of the equivalent load impedance. Hence, a change in the rectified voltage can be used to modify the equivalent load resistance R_L.

IV. Optimization Strategy

In this section, two methods to obtain the maximum efficiency for a desired amount of output power are presented. The first approach is based on the numerical optimization of the efficiency for a given output power using the resistive and reactive part of the equivalent load impedance. Since it is not straightforward to obtain the values of R_L and X_L during steady state, a second optimization method is introduced, where the rectifier input current I_L is optimized as a function of the phase-shift φ and the rectified voltage V_r. These two measurable parameters can be used to achieve the maximum efficiency of the system for every value of the output power. It is worth noting that both presented optimization methods yield the same performance. Additionally, simulation results of the proposed concept are presented and compared to other state-of-the-art optimization approaches. The different possibilities discussed in this paper to optimize the load impedance are summarized in Table I.

A. Optimization of the Resistive and Reactive Part

By controlling the resistive as well as the reactive part of the equivalent load impedance it is possible to optimize the system efficiency for a desired value of the output power. In order to calculate the optimum load impedance a constrained optimization process for every desired value of the output power is used. Mathematically, this constrained optimization can be formulated as

$$Z_{L,opt}(P_{out}) = \arg\max_{R_L, X_L} \left(\eta(R_L, X_L)\,|_{P_{out}}\right) \qquad (13)$$

which can be numerically solved with an appropriate software tool, e.g., with MATLAB. Fig. 6 presents the results of the constrained optimization process in (13) at a constant operating frequency of 140 kHz for a relatively high coupling factor $k = 0.6$ and a low coupling factor of $k = 0.3$. The plots compare the impedance behavior as well as the achieved efficiency of the maximum power approach (conjugate matching of load and output impedances $Z_L = Z_o^*$ and optimizing R_L), the synchronous rectification approach (purely resistive R_L) and the proposed approach (optimizing both, the resistive and the reactive part). Additionally, the point of maximum efficiency, obtained with the single-point optimization approach ($R_L = R_{L,opt}, X_L = -X_s$), is marked in the plots. Fig. 6(a) and (b) illustrates the behavior of the resistive and the reactive part, respectively, over the output power for a tightly coupled system $(k = 0.6)$. The efficiency of the different approaches in dependence on the output power is shown in Fig. 6(c). Fig. 6(d)–(f) presents the results for the same system with a lower coupling factor $k = 0.3$.

The variation of the phase-shift adds an additional degree of freedom for the proposed control method, thus achieving an increased overall efficiency and a higher power transfer capability when compared to the conventional optimization approaches. For tight coupling $(k = 0.6)$, the synchronous rectification achieves a lower system efficiency in the low power region as well as at the end of the medium power range when compared to the proposed method. Additionally, the maximum amount of extracted power is limited when using synchronous rectification while the presented method is able to obtain the maximum possible output power. When utilizing the maximum power approach, the results show a considerably lower efficiency over the whole operating range compared to the optimized concept. If the output power is increased, the optimal values of R_L and X_L are approaching the values of the maximum power method. At the point of maximum power both approaches yield the same values for the optimal resistive and reactive part of the system. Canceling the reactive part (single-point optimization) achieves the maximum efficiency only for a single point of output power. At this point the obtained values for R_L and X_L are the same as for the proposed concept. On the other hand, for different values of output power the efficiency is significantly reduced when compared to the proposed method.

For a system with a lower coupling factor $k = 0.3$ the benefit of the proposed concept in terms of efficiency gain and higher power transfer capability significantly increases when compared to a synchronous rectification approach, as shown in Fig. 6(d)–(f). The simulation results clearly highlight the achievable advantage in performance of the proposed concept by increasing

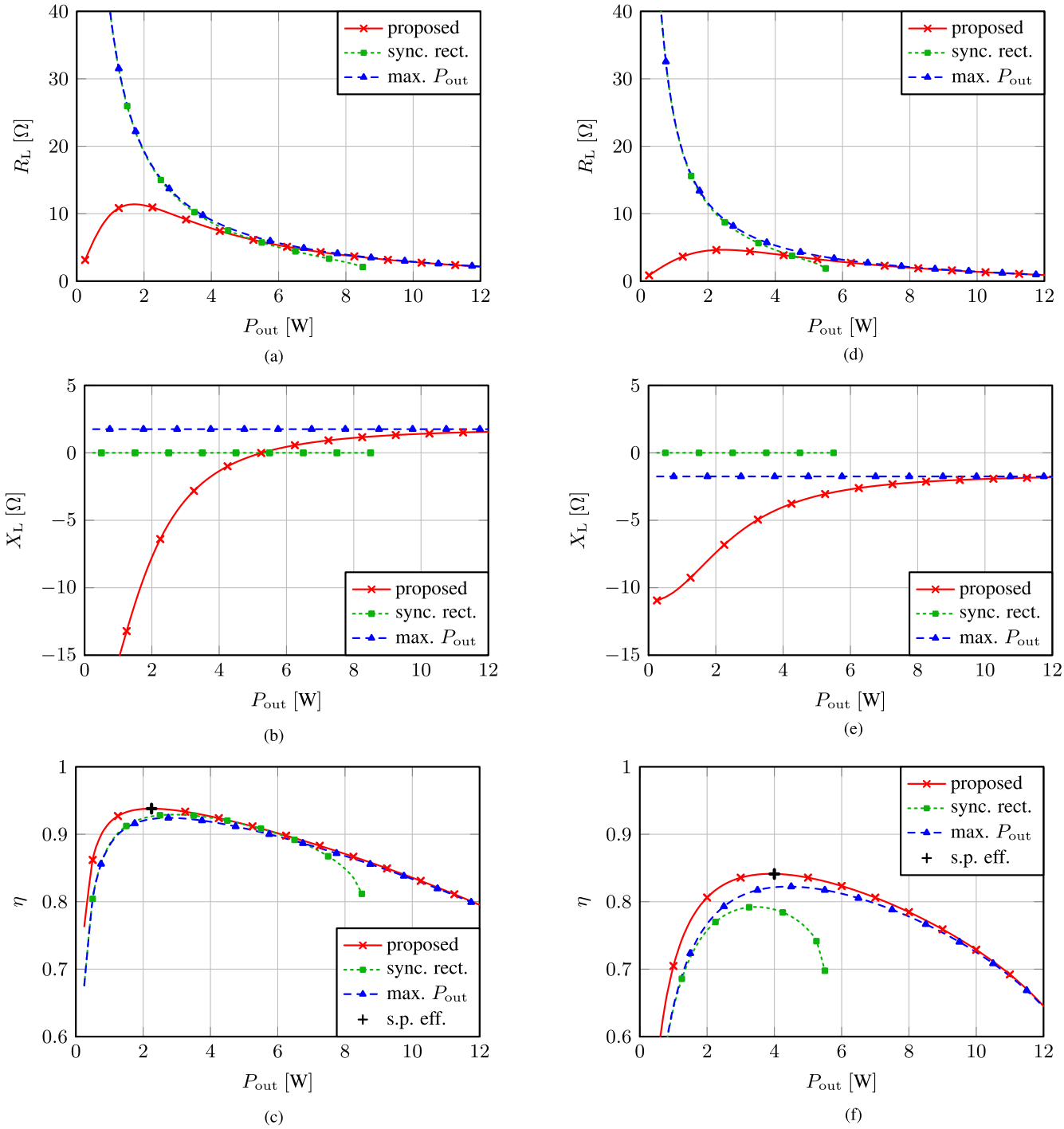

Fig. 6. Impedance behavior and efficiency of the proposed concept compared to the maximum power approach and a synchronous rectifier. (a) Resistive part R_{L} over output power P_{out} for $k = 0.6$. (b) Reactive part X_{L} over output power P_{out} for $k = 0.6$. (c) Efficiency η over output power P_{out} for $k = 0.6$. (d) Resistive part R_{L} over output power P_{out} for $k = 0.3$. (e) Reactive part X_{L} over output power P_{out} for $k = 0.3$. (f) Efficiency η over output power P_{out} for $k = 0.3$.

the efficiency for the same amount of output power and pushing the power transfer capability of the system.

B. Optimization of the Phase-Shift and Rectified Voltage

This section introduces a second possibility to solve the constrained optimization problem in (13) based on measurable system parameters. In this approach, the optimal rectifier input current $I_{\text{L,opt}}$ and the optimal load impedance $Z_{\text{L,opt}}$ in dependence on the phase-shift φ and the rectified voltage V_{r} are derived to obtain the highest possible system efficiency for every value of the desired output power. Additionally, simulation results are presented and compared to experimental results. To obtain the optimal system parameters, the system in Fig. 2

is represented as a two-port network which can be denoted in matrix form as

$$\begin{pmatrix} I_\mathrm{p} \\ V_\mathrm{L} \end{pmatrix} = \begin{pmatrix} Y_{11} & A_{12} \\ A_{21} & -Z_{22} \end{pmatrix} \begin{pmatrix} V_\mathrm{in} \\ I_\mathrm{L} \end{pmatrix} \tag{14}$$

where the gain $A_{12} = A_{21}$ represents the ratio of the input current I_p to the output current I_L if the primary side is shorted, respectively the ratio of the secondary side voltage V_L to the primary side voltage V_in in case the secondary side is open. A_{12} can be calculated by

$$A_{12} = \frac{jX_\mathrm{m}}{R_\mathrm{p} + j(X_\mathrm{p} + X_\mathrm{m})}. \tag{15}$$

The impedance Z_{22} represents the output impedance of the wireless link in case the primary side is shorted, it can be derived as

$$Z_{22} = Z_\mathrm{s} + \frac{jX_\mathrm{m}Z_\mathrm{p}}{R_\mathrm{p} + j(X_\mathrm{p} + X_\mathrm{m})}. \tag{16}$$

In order to calculate the optimum value of the impedance for every value of the output power an analytic solution for the constrained optimization process in (13) has been derived based on Lagrangian optimization methods. Since the efficiency is defined as the ratio between the input and output power, and P_out is a fixed value during the optimization process, the efficiency can be maximized by minimizing the input power P_in. Hence, the objective and the constraint for the Lagrangian optimization can be denoted by

$$P_\mathrm{in} = \mathrm{Re}\{V_\mathrm{in}^* I_\mathrm{p}\} = V_\mathrm{in}\mathrm{Re}\{I_\mathrm{p}\} \tag{17}$$

$$P_\mathrm{out} = \mathrm{Re}\{V_\mathrm{L}^* I_\mathrm{L}\} = \text{constant} \tag{18}$$

respectively, where the phase of the input voltage V_in is referenced as 0° during the calculations, and hence V_in is purely real. For the proposed system a constant input voltage V_in, a constant coupling factor k and a constant operating frequency are assumed and hence the input power in (17) can be optimized by minimizing the primary side current I_p. After solving the constrained optimization problem in (17) and (18), the optimized output current $I_{\mathrm{L,opt}}(P_\mathrm{out}, V_\mathrm{in}) = I^\mathrm{R}_{\mathrm{L,opt}}(P_\mathrm{out}, V_\mathrm{in}) + jI^\mathrm{I}_{\mathrm{L,opt}}(P_\mathrm{out}, V_\mathrm{in})$ for a given amount of output power and a constant input voltage can be calculated as

$$I^\mathrm{R}_{\mathrm{L,opt}}(P_\mathrm{out}, V_\mathrm{in}) = V_\mathrm{in} \frac{\mathrm{Re}\{A_{12}\}\left[-\sqrt{1 - \frac{4P_\mathrm{out}\mathrm{Re}\{Z_{22}\}}{V_\mathrm{in}^2|A_{12}|^2}} + 1\right]}{2\mathrm{Re}\{Z_{22}\}} \tag{19}$$

$$I^\mathrm{I}_{\mathrm{L,opt}}(P_\mathrm{out}, V_\mathrm{in}) = V_\mathrm{in} \frac{\mathrm{Im}\{A_{12}\}\left[1 + \sqrt{1 - \frac{4P_\mathrm{out}\mathrm{Re}\{Z_{22}\}}{V_\mathrm{in}^2|A_{12}|^2}}\right]}{2\mathrm{Re}\{Z_{22}\}} \tag{20}$$

where $I^\mathrm{R}_{\mathrm{L,opt}}$ denotes the real and $I^\mathrm{I}_{\mathrm{L,opt}}$ the imaginary part of the current $I_{\mathrm{L,opt}}$. With (19) and (20) the optimum equivalent load impedance to achieve the maximum efficiency for a given amount of output power can be derived as

$$Z_{\mathrm{L,opt}}(P_\mathrm{out}, V_\mathrm{in}) = \frac{A_{12}V_\mathrm{in}}{I_{\mathrm{L,opt}}(P_\mathrm{out}, V_\mathrm{in})} - Z_{22}. \tag{21}$$

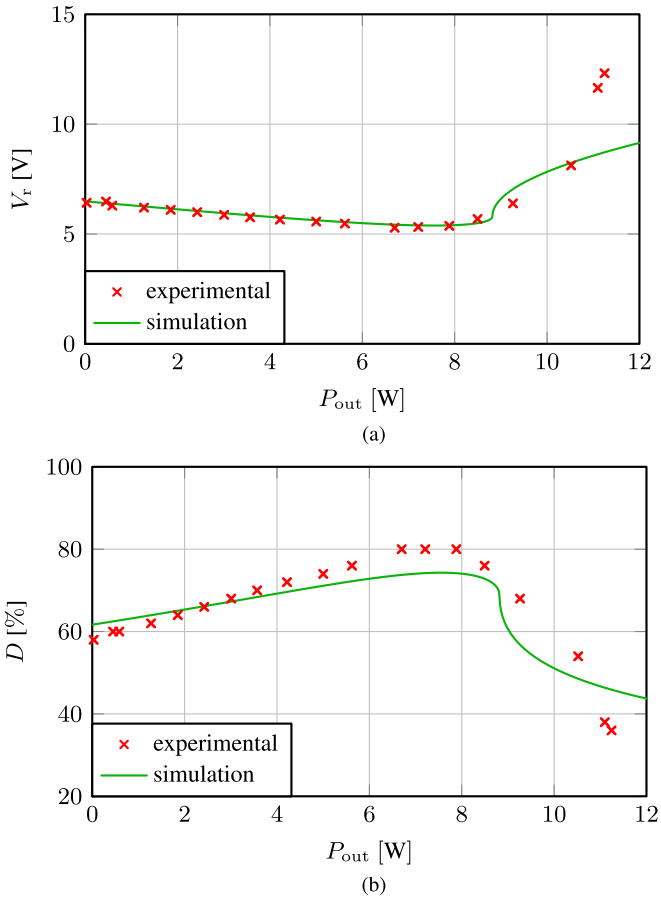

Fig. 7. Comparison of the simulation results with the measured values of the experimental setup. (a) Rectified voltage V_r as a function of the output power P_out. (b) Duty cycle D of the dc–dc converter over output power P_out.

In order to calculate the optimal values of the rectified voltage V_r and the phase-shift φ, (10) has to be solved at the point of optimal impedance $Z_\mathrm{L} = Z_{\mathrm{L,opt}}$, which gives

$$V_\mathrm{r}(Z_{\mathrm{L,opt}}) = \frac{\pi\sqrt{2}}{4}\left|(A_{21}V_\mathrm{in} - Z_{22}I_{\mathrm{L,opt}})\right| \tag{22}$$

$$\varphi(Z_{\mathrm{L,opt}}) = -\arg\left[\frac{\pi\sqrt{2}}{4}(A_{21}V_\mathrm{in} - Z_{22}I_{\mathrm{L,opt}})\right]. \tag{23}$$

With the rectified voltage in (22), and if the dc output voltage V_ℓ at the battery is assumed to be constant, the optimal duty cycle D of an idealized dc–dc converter can be derived as

$$D(Z_{\mathrm{L,opt}}) = \frac{V_\ell}{|V_\mathrm{r}(Z_{\mathrm{L,opt}})|}. \tag{24}$$

The values of the rectified voltage V_r and the duty cycle D of the dc–dc converter are measurable on the prototyping system during steady-state operation. Hence, the point of maximum efficiency for every value of output power can be obtained on hardware and compared to the theoretical results. Fig. 7(a) shows a comparison of the simulation results of V_r obtained from (22) to the measurement results of the developed prototyping system. Fig. 7(b) compares the simulations according to (24) and the

experimental results of the duty cycle D as a function of the output power P_{out}.

Fig. 7(a) shows that the value of the rectified voltage V_{r} is decreasing till an output power of about 8 W. At that point the maximum of the optimal phase-shift is reached and the rectified voltage begins to rise again. Hence, there is a large range of output power values where the rectified voltage only changes marginally, which can be exploited in an optimal control concept. The acquired experimental results are in good agreement with the simulations, especially in the low to medium power range up to 8 W.

In Fig. 7(b) the duty cycle D increases up to an output power of around 8 W. Then it starts to decrease since the maximum value of the optimal phase-shift is reached. Simulations and experimental results again match quite well, a major reason for the deviations is the fact that an ideal model of a dc–dc converter is assumed and the converter efficiency is not considered in the derived analytical equations for simplicity.

V. Experimental Results

This section provides detailed information about the experimental setup and the system parameters used for the measurements. Furthermore, the acquired measurement results using the proposed concept are compared to a synchronous rectifier solution.

A. Prototyping Setup

To verify the results obtained by the simulations an IPT prototyping system has been designed based on the Qi standard specifications [11]. The system is intended to operate at frequencies between 110 and 205 kHz with a resonance frequency of $f_{\mathrm{res}} = 100$ kHz. For the following measurements, a dc supply voltage of $V_{\mathrm{s}} = 19$ V and a constant operating frequency of $f_{\mathrm{op}} = 140$ kHz is used. The primary side inductor L_{p}[28] with an outer diameter of 43 mm is driven by an inverter stage, switching at the operating frequency of the system. The secondary side inductor L_{s} [29] with an outer diameter of 28 mm is placed at a distance of 3 mm from the primary side, resulting in a measured coupling factor of $k = 0.6$. For the low coupling factor measurements the distance between the inductors has been increased to 10 mm, yielding a measured coupling factor of $k = 0.3$. At the secondary side an active rectifier is utilized to rectify the induced ac voltage, and an output capacitor $C_{\mathrm{r}} = 22$ μF is used for stabilizing the rectified voltage. A dc–dc converter, designed for constant-current constant-voltage charging operation, is connected at the output of the rectifier to charge the battery. At the output of the system, a special battery emulation equipment [30] has been attached, and its parameters have been adjusted to simulate the typical behavior of a lithium-ion battery [31]. The digital control of the whole wireless charging system has been implemented on an external field programmable gate array (FPGA) board [32]. A schematic overview of the entire prototyping system is shown in Fig. 8, and a summary of the main system parameters is given in Table II.

To validate the proposed concept, the controller of the primary and secondary side is implemented on an FPGA which controls the switches of the inverter stage $(Q_1 - Q_2)$ as well as the active rectifier $(S_1 - S_4)$ and the dc–dc converter $(T_1 - T_2)$. In the current prototyping system, which is intended to demonstrate the advantages of the proposed concept, the phase-shift φ between I_{L} and V_{L} is realized by inserting a time delay between the primary and secondary side control signals. To achieve this, a communication link between the primary and secondary side controller has been assumed. The current controller implementation operates in open loop. The calculated optimal values are used as initial conditions, and then the control parameters φ and D are iteratively adjusted to compensate for parameter variations and to achieve optimal system performance. The higher the uncertainty of the system parameters, the less accurate are the calculated results of the optimum operation conditions.

B. Experimental Results

In order to validate the proposed concept, the values of the phase-shift φ and the rectified voltage V_{r}, which is controlled by the duty cycle D of the dc–dc converter, have been adjusted during the measurements to achieve maximum efficiency for each value of the output power. For the synchronous rectification, a zero-crossing detection of the rectifier input current I_{L} is implemented and the full bridge $(S_1 - S_4)$ is driven accordingly. The duty cycle D of the dc–dc converter is used to control the equivalent load resistance and hence the amount of power at the output of the system.

When utilizing the proposed optimization method for a coupling factor $k = 0.6$, the measured point of maximum efficiency $\eta = 77.3\%$ is reached at an output power of $P_{\mathrm{out}} = 3$ W with a phase-shift $\varphi = 20^{\circ}$ and a duty cycle $D = 68\%$. Fig. 9(a) shows a measurement of the waveforms of the rectifier input voltage V_{L} and the input current I_{L} employing these conditions. Fig. 9(b) shows the same waveforms for the synchronous rectification approach using comparable conditions as in Fig. 9(a) (duty cycle $D = 66\%$, output power $P_{\mathrm{out}} = 2.8$ W and efficiency $\eta = 75.9\%$).

As shown in Fig. 9, the proposed control method introduces a phase-shift between the input current I_{L} and the input voltage V_{L} of the active rectifier, while the synchronous rectification maintains a zero phase-shift behavior of the system.

In Fig. 10 the measurement results of the system efficiency as a function of the output power P_{out} are shown for tightly coupled inductors ($k = 0.6$), and for a system with relatively low coupling ($k = 0.3$). The plots compare the performance of the proposed control method to a conventional synchronous rectification approach. For the presented optimization concept, the phase-shift and the duty cycle have been controlled and for the synchronous rectification only the duty cycle has been adjusted during the measurement.

The experimental results show comparable trends as the simulations in Fig. 6, namely the proposed control strategy always achieves the same or a higher efficiency than a synchronous rectification approach. For a coupling factor $k = 0.6$ the efficiency of the examined system can be increased in the low power range (up to 4 W) yielding, e.g., an efficiency of 75% at an output power of $P_{\mathrm{out}} = 1.8$ W compared to an efficiency of 71.2% for synchronous rectification. In the medium power range, between 4 and 7 W the efficiency does not increase significantly in

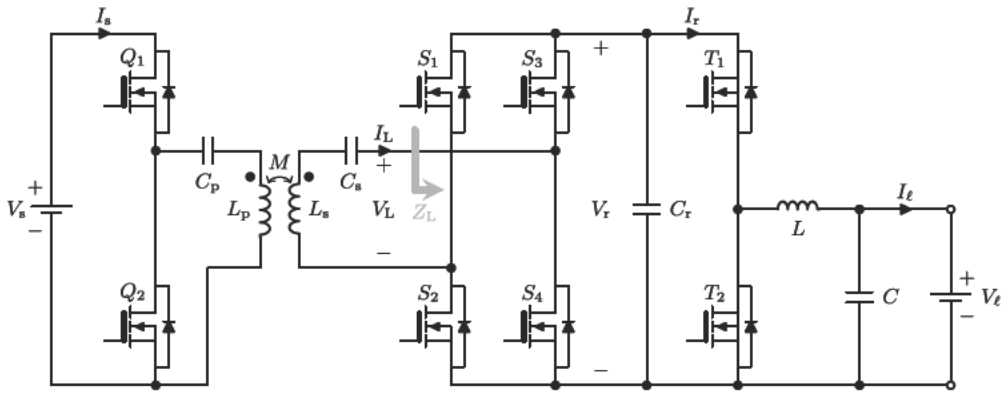

Fig. 8. Schematic illustration of the experimental setup. The discrete MOSFETs are controlled by an FPGA which implements the digital control architecture.

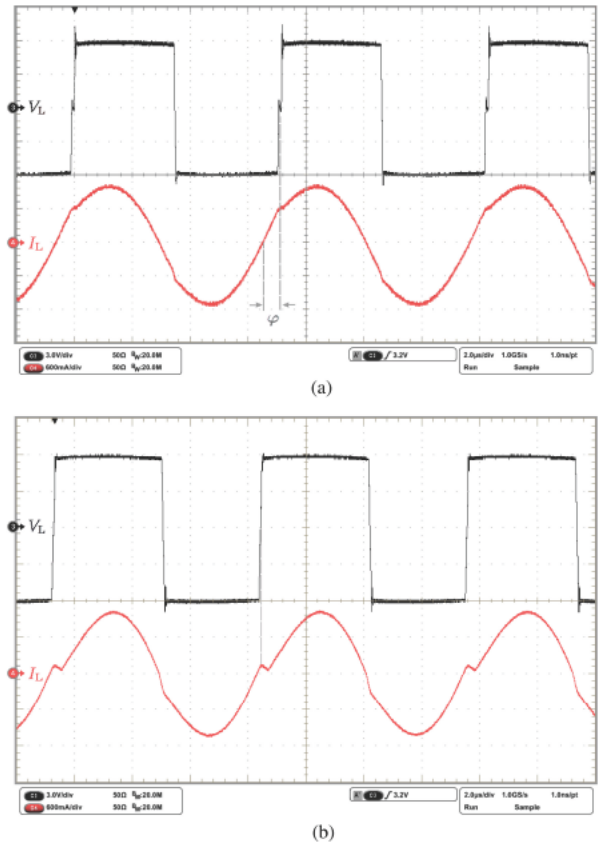

Fig. 9. Measurement of the key system waveforms for the proposed concept and a synchronous rectification approach at $k = 0.6$. (a) Waveforms of the rectifier input voltage V_L (3V/div) and input current I_L (600 mA/div) for the proposed concept with a phase-shift of $\varphi = 20°$ and a duty cycle $D = 68\%$. (b) Waveforms of V_L (3V/div) and I_L (600 mA/div) for synchronous rectification with a duty cycle $D = 66\%$.

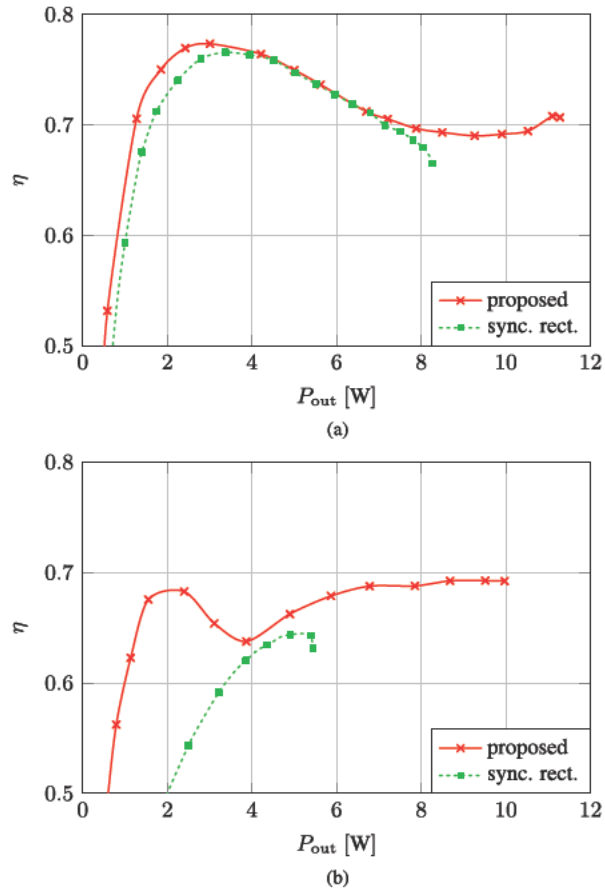

Fig. 10. Experimental results of the overall system efficiency η for the proposed concept compared to a synchronous rectifier solution as a function of the output power P_{out}. (a) Measurement results for tightly coupling $k = 0.6$. (b) Measurement results for a low coupling factor $k = 0.3$.

comparison to a synchronous rectifier. In case the output power is further increased, the proposed control method is again able to achieve a higher efficiency yielding, e.g., an efficiency of 69.4% at an output power $P_{out} = 8.2$ W compared to an efficiency of 66.4% with synchronous rectification. Furthermore, the amount of output power which can be extracted by the synchronous rectifier is limited to $P_{out} = 8.26$ W. A further increase of the input power P_{in} yields lower values of the output power P_{out} due to the decrease in efficiency. In contrast, the proposed concept is able to extend the achievable output power of the system to 11.24 W, thus increasing the maximum achievable output power by 36%, while maintaining a high efficiency. For a lower coupling factor of $k = 0.3$ an even higher performance increase in terms of efficiency and extractable power can be obtained. The maximum output power of the system could be increased from 5.4 to 9.9 W (by 83%) when compared to a synchronous

rectification approach. Additionally, at every point of the operating range the achieved efficiency of the proposed approach is higher than for synchronous rectification. The measurement results of the prototyping setup clearly highlight the possibility of the proposed concept to extract more power while improving the efficiency of the system in comparison to a synchronous rectifier solution.

VI. Conclusion

In this study, a concept to achieve optimal efficiency for a desired amount of output power as well as to extend the power transfer capability of IPT systems has been presented. The proposed method is based on the adjustment of the equivalent load impedance as a function of the output power, which can be realized by introducing a phase-shift between current and voltage in the active rectifier, and by controlling the level of the rectified voltage. When operating exactly at resonance frequency the optimal equivalent impedance is purely resistive, and consequently the proposed approach behaves like a synchronous rectifier. If any deviation of the resonance frequency occurs, e.g., caused by parameter variations of the passive components, the presented concept achieves a superior performance.

The theoretical background of the proposed concept has been presented and validated by simulations as well as by experiments with the help of a WPT prototyping system based on the Qi standard. The results show that the efficiency of the system can be increased over the whole measurement range when compared to a synchronous rectifier. The performance gain increases for decreasing coupling factors. Furthermore, the maximum extractable output power of the prototyping system is raised by 36% for a coupling factor $k = 0.6$, and even by 83% for a coupling factor of $k = 0.3$, again in comparison to a synchronous rectification approach.

References

[1] A. RamRakhyani, S. Mirabbasi, and M. Chiao, "Design and optimization of resonance-based efficient wireless power delivery systems for biomedical implants," *IEEE Trans. Biomed. Circuits Syst.*, vol. 5, no. 1, pp. 48–63, Feb. 2011.

[2] M. Zargham and P. Gulak, "Maximum achievable efficiency in near-field coupled power-transfer systems," *IEEE Trans. Biomed. Circuits Syst.*, vol. 6, no. 3, pp. 228–245, Jun. 2012.

[3] R. Wu, W. Li, H. Luo, J. Sin, and C. Yue, "Design and characterization of wireless power links for brain machine interface applications," *IEEE Trans. Power Electron.*, vol. 29, no. 10, pp. 5462–5471, Oct. 2014.

[4] G. Covic and J. Boys, "Modern trends in inductive power transfer for transportation applications," *IEEE J. Emerg. Sel. Topics Power Electron.*, vol. 1, no. 1, pp. 28–41, Mar. 2013.

[5] S. Lukic and Z. Pantic, "Cutting the cord: Static and dynamic inductive wireless charging of electric vehicles," *IEEE Electrific. Mag.*, vol. 1, no. 1, pp. 57–64, Sep. 2013.

[6] S. Choi, J. Huh, W. Lee, and C. Rim, "Asymmetric coil sets for wireless stationary EV chargers with large lateral tolerance by dominant field analysis," *IEEE Trans. Power Electron.*, vol. 29, no. 12, pp. 6406–6420, Dec. 2014.

[7] S. Hui and W. Ho, "A new generation of universal contactless battery charging platform for portable consumer electronic equipment," *IEEE Trans. Power Electron.*, vol. 20, no. 3, pp. 620–627, May 2005.

[8] E. Waffenschmidt, "Wireless power for mobile devices," in *Proc. IEEE Int. Telecom. Energy Conf.*, 2011, pp. 1–9.

[9] A. Satyamoorthy, P. Riehl, H. Akram, Y.-C. Yen, J.-C. Yang, B. Juan, C.-M. Lee, and F.-C. Lin, "Wireless power receiver for mobile devices supporting inductive and resonant operating modes," in *Proc. IEEE Wireless Power Transfer Conf.*, 2014, pp. 52–55.

[10] S. Hui, W. Zhong, and C. Lee, "A critical review of recent progress in mid-range wireless power transfer," *IEEE Trans. Power Electron.*, vol. 29, no. 9, pp. 4500–4511, Sep. 2014.

[11] (2015). The wireless power consortium (WPC) website [Online]. Available: http://www.wirelesspowerconsortium.com/

[12] (2015). The alliance for wireless power (A4WP) website [Online]. Available: http://www.rezence.com/

[13] T. Imura and Y. Hori, "Maximizing air gap and efficiency of magnetic resonant coupling for wireless power transfer using equivalent circuit and neumann formula," *IEEE Trans. Ind. Electron.*, vol. 58, no. 10, pp. 4746–4752, Oct. 2011.

[14] S. Kong, M. Kim, K. Koo, S. Ahn, B. Bae, and J. Kim, "Analytical expressions for maximum transferred power in wireless power transfer systems," in *Proc. IEEE Int. Symp. Electromagn. Compatibility*, 2011, pp. 379–383.

[15] W. Zhang, S.-C. Wong, C. K. Tse, and Q. Chen, "Design for efficiency optimization and voltage controllability of series-series compensated inductive power transfer systems," *IEEE Trans. Power Electron.*, vol. 29, no. 1, pp. 191–200, Jan. 2014.

[16] Y. Zhang, Z. Zhao, and K. Chen, "Frequency decrease analysis of resonant wireless power transfer," *IEEE Trans. Power Electron.*, vol. 29, no. 3, pp. 1058–1063, Mar. 2014.

[17] W. P. Choi, W. C. Ho, X. Liu, and S. Y. R. Hui, "Comparative study on power conversion methods for wireless battery charging platform," in *Proc. IEEE Int. Power Electron. Motion Control Conf.*, 2010, pp. 9–16.

[18] D. Huwig and P. Wambsganss, "Digitally controlled synchronous bridge-rectifier for wireless power receivers," in *Proc. IEEE Appl. Power Electron. Conf. Expo.*, 2013, pp. 2598–2603.

[19] M. Galizzi, M. Caldara, V. Re, and A. Vitali, "A novel Qi-standard compliant full-bridge wireless power charger for low power devices," in *Proc. IEEE Wireless Power Transfer Conf.*, 2013, pp. 44–47.

[20] Y. Moriwaki, T. Imura, and Y. Hori, "Basic study on reduction of reflected power using DC/DC converters in wireless power transfer system via magnetic resonant coupling," in *Proc. IEEE Int. Telecom. Energy Conf.*, 2011, pp. 1–5.

[21] J. Bird, *Electrical Circuit Theory and Technology*. Oxford, U.K.: Elsevier, 2003.

[22] T. Nishiyama and Y. Saitoh, "Wireless power receiver, wireless power transmission system, and power controller," U.S. Patent 2012/0 223 587 A1, Sep. 6, 2012.

[23] C. Zhao, Z. Wang, J. Du, J. Wu, S. Zong, and X. He, "Active resonance wireless power transfer system using phase shift control strategy," in *Proc. IEEE Appl. Power Electron. Conf. Expo.*, 2014, pp. 1336–1341.

[24] A. Berger, M. Agostinelli, S. Vesti, J. A. Oliver, J. A. Cobos, and M. Huemer, "Phase-shift and amplitude control for an active rectifier to maximize the efficiency and extracted power of a wireless power transfer system," in *Proc. IEEE Appl. Power Electron. Conf. Expo.*, 2015, pp. 1620–1624.

[25] E. Bou, R. Sedwick, and E. Alarcon, "Maximizing efficiency through impedance matching from a circuit-centric model of non-radiative resonant wireless power transfer," in *Proc. IEEE Int. Symp. Circuits Systems*, 2013, pp. 29–32.

[26] M. Kiani and M. Ghovanloo, "The circuit theory behind coupled-mode magnetic resonance-based wireless power transmission," *IEEE Trans. Circuits Syst. I*, vol. 59, no. 9, pp. 2065–2074, Sep. 2012.

[27] R. Erickson and D. Maksimović, *Fundamentals of Power Electronics*. Boston, MA, USA: Springer, 2001.

[28] Wurth Elektronik, 760308101 WE-WPCC wireless power charging coil datasheet. (2015). [Online]. Available: http://katalog.we-online.de/pbs/datasheet/760308101.pdf

[29] Wurth Elektronik, 760308201 WE-WPCC wireless power charging coil datasheet. (2015). [Online]. Available: http://katalog.we-online.de/pbs/datasheet/760308201.pdf

[30] Agilent Technologies, N6781A 2-quadrant source/measure unit for battery drain analysis. (2015). [Online]. Available: www.agilent.com/find/n6781

[31] M. Chen and G. Rincon-Mora, "Accurate electrical battery model capable of predicting runtime and IV performance," *IEEE Trans. Energy Convers.*, vol. 21, no. 2, pp. 504–511, Jun. 2006.

[32] Terasic Technologies Inc. *DE2-115 development and education board, user manual*. (2015). [Online]. Available: http://www.altera.com/education/univ/materials/boards/de2-115/unv-de2-115-board.html